JAERI-M
8429

ICRF HEATING IN DIVA : PARAMETER SURVEY AND VERY HIGH EFFICIENCY ION HEATING EXPERIMENT

September 1979

Haruyuki KIMURA, Kazuo ODAJIMA, Seio SENGOKU,
Satoru IIZUKA,* Tatsuo SUGIE, Koki TAKAHASHI,
Toshihiko YAMAUCHI, Katsuaki KUMAGAI
Hiroshi TAKEUCHI, Hiroshi MATSUMOTO,
Toshiaki MATSUDA, Kazumi OHASA,
Masayuki NAGAMI, Shin YAMAMOTO,
Takashi NAGASHIMA, Hikosuke MAEDA and
Yasuo SHIMOMURA

日 本 原 子 力 研 究 所
Japan Atomic Energy Research Institute

JAERI-M 8429

ICRF Heating in DIVA : Parameter Survey and Very High Efficiency Ion Heating Experiment

Haruyuki KIMURA, Kazuo ODAJIMA, Seio SENGOKU, Satoru IIZUKA*, Tatsuo SUGIE, Koki TAKAHASHI, Toshihiko YAMAUCHI, Katsuaki KUMAGAI, Hiroshi TAKEUCHI, Hiroshi MATSUMOTO, Toshiaki MATSUDA, Kazumi OHASA, Masayuki NAGAMI, Shin YAMAMOTO, Takashi NAGASHIMA, Hikosuke MAEDA and Yasuo SHIMOMURA

Division of Thermonuclear Fusion Research,
Tokai Research Establishment, JAERI

(Received August 16, 1979)

ICRF Heating of impurity-free tokamak plasmas has been studied in DIVA. The frequency is fixed at 25 MHz, which is a second harmonic cyclotron frequency of deuterons with a toroidal magnetic field of 16.4 kG. (1) Optimum heating conditions were investigated in varying the toroidal magnetic field B_T and the proton-to-deuteron density ratio ε_p. The most favorable ion heating is observed for $B_T \sim 18$ kG and $\varepsilon_p = 5 \sim 10\%$; which is explained by two-ion hybrid effects. (2) In heating results after improvement of the coupling structure, the ion heating efficiency is raised from 40% to almost 100%. Bulk ion temperature increased by a factor of 2.7 in application of the rf net power of 180 kW including the circuit loss.

Keywords: DIVA Tokamak, Heating Efficiency, ICRF Heating, Two-ion Hybrid effect, Ion Temperature

---

*) On leave from University of Tohoku, Sendai Japan

DIVAに於けるICRF加熱：パラメーターサーベイと超高能率イオン加熱実験

日本原子力研究所東海研究所核融合研究部
木村　晴行・小田島和男・仙石　盛夫
飯塚　　哲*・杉江　達夫・高橋　興起
山内　俊彦・熊谷　勝昭・竹内　　浩
松本　　宏・松田　俊明・大麻　和美
永見　正幸・山本　　新・永島　　孝
前田　彦祐・下村　安夫

（1979年8月16日受理）

DIVAに於いて不純物の影響が極めて少ないトカマクプラズマに対するICRF加熱の研究がなされた。周波数は25 MHz（固定）であり，これはトロイダル磁場16.4 kGに対する重水素の2倍のサイクロトロン周波数に相当する。(1)トロイダル磁場B_T及び水素と重水素の密度比ε_Pを変化させることにより最適な加熱条件が調べられた。最も有効なイオン加熱はB_T～18 KG，ε_P＝5～10％の場合に観測される。この結果はイオン—イオン・ハイブリッド効果によって説明される。(2)結合系に対して改良が施され，改良後の実験結果が次に述べられる。イオンの加熱効率は40％からほぼ100％へ増加し，イオン温度は180 kWのrfパワー（回路損失を含めて）の印加により約2.7倍に上昇した。

＊特別研究生　東北大学工学部

CONTENTS

目　　次

1. Introduction

This paper describes high frequency wave heating in the ion cyclotron range of frequency (ICRF) in DIVA tokamak[1], using a second harmonic cyclotron frequency of deuterium for a $D^+ + H^+$ discharge, where the latter is a minority component. ICRF heating has been intensively investigated in several tokamaks, i.e. early experiments in TO-1[2], TM-1-Vch[3], ST[4], and recent experiments in TFR[5], TM-1-VCh[6], T-4[7], ATC[8], etc. Those experiments were mainly performed for a deuterium plasma with a minority proton component, using a second harmonic cyclotron frequency of deuterium. Wave damping mechanisms have been also investigated in theory [9,10,11]. In TFR, it was shown that variation of wave amplitude versus major radius location of a harmonic cyclotron resonance layer of deuteron in a plasma crosssection was asymmetric with respect to a plasma center[5]. This asymmetry was well explained by the theory of mode conversion of the magnetosonic wave at the two-ion hybrid resonance layer[9,11]. In addition, it was reported, preliminary as it was, that heating efficiency was dependent on the amount of proton component, that is, ion temperature increase ΔT_i associated with the rf pulse was reduced to 50% when the amount of H^+ was increased from 8 to 20%, which again agreed with mode conversion theory[12].

Thus, it is generally recognized that heating mechanism of ICRF heating using a second harmonic cyclotron frequency of deuterium for a $D^+ + H^+$ discharge is due to the mode conversion of the magnetosonic wave at the two-ion hybrid resonance layer. However details of heating mechanism have not yet been known because of a lack of reliable information of the ratio of proton to deuteron density during rf pulse as well as impurity effects. In rf heating experiment it is indispensable to keep impurity influxes as small as possible when rf pulse is applied, in order to exclude a possibility of plasma heating due to impurities. Assuming $Z_{eff} = 4$ and oxygen impurities, more than 10% of oxygen are present in a $D^+ + H^+$ plasma. In this situation the effects of O^{8+} and O^{7+} must be taken into account. In addition, if the first wall is not conditioned well, electron density and and amount of impurity influxes increase on applying rf pulse. Then ΔT_i associated with rf pulse is partly due to the increase of Joule input with the increase of impurity influxes. In our preliminary experiment[18], where the first wall was not conditioned well, one turn loop voltage as well as ion temperature increased significantly on applying rf pulse of 70J.

Similar increase of ion temperature was observed by neon injection instead of rf pulse.

Now the first wall of DIVA was thoroughly flushed by titanium. Extremely pure plasma was obtained i.e. $Z_{eff} \simeq 1$. Radiation loss was less than 10 KW for the Joule input of 85 KW. One turn loop voltage V_L and electron density were not affected in the experiment with supplying rf net energy 1 KJ. A limit has not been found for the rf net energy up to now.

In Sec. 2 we examined the dependence of charge exchange neutral energy spectrum on the toroidal field B_T and the ratio of proton to deuteron density ε_p over the ranges of $12 \leq B_T \leq 19$ KG and $2 \leq \varepsilon_p \leq 40\%$, respectively. ε_p was measured during rf pulse by spectroscopy. The most appropriate conditions of B_T and ε_p were found out, in which the maximum bulk ion heating occurred, no high energy tail was present and no adverse effect on the plasma confinement was observed.

Heating efficiency, however, was only up to 40%. The rest of the rf power went to the edge plasma by an electrostatic coupling between the antenna and the plasma surrounding it. In Sec. 3 we report experimental results using an improved coupling structure with an electrostatic Faraday shield. Heating efficiency of about 100% was obtained.

2. Parameter survey for the optimum ion heating

2.1 Experimental Set-up

The generator was operated at 25 MHz which is a cyclotron frequency for hydrogen ω_{CH} or the second harmonic cyclotron frequency for deuterium $2\omega_{CD}$ at 16.4 KG. Rf power can be up to 200 KW. Figure 1 shows a cross-sectional view of DIVA together with a launching structure (antenna), a matching network and a transmission line. The launching structure was made of a half turn copper strip, 2 × 0.3 cm in cross-section 10.4 cm in radius, and a ceramic cover, 3.5 × 1.5 cm in cross-section 10 cm in inner radius. The launching structure was placed in the shell gap and protected by a pair of molybdenum guard limiters (not shown in Fig. 1) which prevent the ceramic cover from direct contact with the plasma. A Faraday shield was not used for the present experiment.

The rf power was transmitted through a co-axial cable (RG-19U) from the generator to a two stub matching network. The rf power was monitored by a directional coupler in front of the matching network. Coil current was measured by a current probe placed near at the mid-point of the antenna.

Similar increase of ion temperature was observed by neon injection instead of rf pulse.

Now the first wall of DIVA was thoroughly flushed by titanium. Extremely pure plasma was obtained i.e. $Z_{eff} \simeq 1$. Radiation loss was less than 10 KW for the Joule input of 85 KW. One turn loop voltage V_L and electron density were not affected in the experiment with supplying rf net energy 1 KJ. A limit has not been found for the rf net energy up to now.

In Sec. 2 we examined the dependence of charge exchange neutral energy spectrum on the toroidal field B_T and the ratio of proton to deuteron density ε_p over the ranges of $12 \leq B_T \leq 19$ KG and $2 \leq \varepsilon_p \leq 40\%$, respectively. ε_p was measured during rf pulse by spectroscopy. The most appropriate conditions of B_T and ε_p were found out, in which the maximum bulk ion heating occurred, no high energy tail was present and no adverse effect on the plasma confinement was observed.

Heating efficiency, however, was only up to 40%. The rest of the rf power went to the edge plasma by an electrostatic coupling between the antenna and the plasma surrounding it. In Sec. 3 we report experimental results using an improved coupling structure with an electrostatic Faraday shield. Heating efficiency of about 100% was obtained.

2. Parameter survey for the optimum ion heating

2.1 Experimental Set-up

The generator was operated at 25 MHz which is a cyclotron frequency for hydrogen ω_{CH} or the second harmonic cyclotron frequency for deuterium $2\omega_{CD}$ at 16.4 KG. Rf power can be up to 200 KW. Figure 1 shows a cross-sectional view of DIVA together with a launching structure (antenna), a matching network and a transmission line. The launching structure was made of a half turn copper strip, 2 × 0.3 cm in cross-section 10.4 cm in radius, and a ceramic cover, 3.5 × 1.5 cm in cross-section 10 cm in inner radius. The launching structure was placed in the shell gap and protected by a pair of molybdenum guard limiters (not shown in Fig. 1) which prevent the ceramic cover from direct contact with the plasma. A Faraday shield was not used for the present experiment.

The rf power was transmitted through a co-axial cable (RG-19U) from the generator to a two stub matching network. The rf power was monitored by a directional coupler in front of the matching network. Coil current was measured by a current probe placed near at the mid-point of the antenna.

The end of the antenna was terminated to the vacuum vessel as shown in Fig. 1. As the length of the antenna is much shorter than a wavelength of 25 MHz in a free space, the coil current measured at the mid-point of the antenna is almost a peak value.

An antenna loading impedance R_s can be calculated from $R_s = \frac{P_f - P_b}{I_c^2}$ (Ω), where P_f, P_b and I_c are incident and reflected powers and coil current, respectively.

Perpendicular ion temperatures were measured with a 10-ch charge exchange neutral particle energy analyser and a Czerny-Terner mounting vacuum monochromator. Both were placed at almost diametrically opposite ports of the antenna. The charge exchange analyser is not capable of discriminating mass differences and its signal contains contributions both from deuterium and hydrogen. Ion temperature profiles can be obtained from the Doppler broadening of impurity lines by scanning the monochromator[13]. Parallel ion temperature were not measured for the present experiment.

Electron temperature and density were measured with a laser scattering and a 2 mm μ-wave interferometer, respectively. In the scrape-off layer, an electrostatic multigrid energy analyzer[14] and a Katsumata (ion sensitive) probe[15] were used to measure parallel and perpendicular ion temperature, respectively.

2.2 Discharge Conditions

The experiment was performed under the following discharge conditions: The toroidal magnetic field B_T was varied from 12 to 19 KG. The ratio of the divertor hoop current to the plasma current was 1.2, where the latter was 32.5 KA with a flat-top in the case of B_T = 18 KG. Deuterium gas was admitted by two fast-acting valves and a programmable d.c. gas feeder.

The ratio of proton to deuteron density ε_p was measured during the discharge by the monochromator, which was varied over the range of 2 ∿ 40% by adjusting the amount of additional hydrogen gas.

Base plasma parameters in the case of B_T = 18 KG were as follows.

central electron temperature	$T_{eo} \sim 330$ eV
central ion temperature	$T_{io} \sim 200$ eV
averaged electron density	$\bar{n}_e \sim 4 \times 10^{13}$ cm^{-3}
one turn loop voltage	$V_L = 2.5$ V
plasma current	$I_p = 32.5$ KA

effective charge number	$Z_{eff} \simeq 1$
major radius	$R = 60$ cm
antenna (limiter) radius	$a_A = 10$ cm

2.3 Experimental Results

The rf power was applied for 3 ∿ 8 ms. The maximum rf net power was 140 KW, limited by breakdown at the antenna. Although breakdown took place, the rf power could be raised gradually from a low level to the maximum power as before. One turn loop voltage did not change even with the application of the maximum rf power. Change of the electron density was also within shot-to-shot reproducibilities of the base plasma, that is, less than 10%. Typical time evolutions of perpendicular ion temperature $T_{i\perp}$, electron line density $\overline{n_e l}$, plasma current I_p, one turn loop voltage V_L and spectral line intensity OVII (1623 Å) are shown in Fig. 2.

2.3.1 Rf measurement

The measurement with the directional coupler and the current probe showed that plasma loading impedance R_s was 6 ∿ 7Ω. This value changed little over the ranges of B_T and ε_p varied in the present experiment. The same measurement in the absence of the plasma gives the circuit loss R_c, which was 1Ω. Then, a coupling efficiency was about 0.85. Rf net power P_{Net} is defined as follows.

$$P_{Net} = \frac{R_s - R_c}{R_s} (P_f - P_b)$$

Figure 3 shows typical signals from the directional coupler indicating square roots of incident and reflected rf powers, the current probe and a magnetic probe located diametrically opposite to the position of the antenna, in the case of $B_T = 18$ KG and $\varepsilon_p = 5 \sim 10\%$. The signal of the magnetic probe shows there is no resonant peak since the two-ion hybrid resonance layer exists in the torus. Figure 4 shows $\tilde{B}_\theta$ as a function of major radius location of a fundamental cyclotron resonance layer for hydrogen, where the frequency was fixed at 25 MHz and $\varepsilon_p = 5 \sim 10\%$. As reported in TFR[5] and ATC[11], wave damping is asymmetric with respect to the plasma center.

2.3.2 Heating experiments

We first examined the response of charge exchange neutral spectra, varying the toroidal field, i.e. the position of the fundamental cyclotron resonance layer for hydrogen. Figure 5 shows some examples of charge exchange neutral spectra and corresponding cyclotron resonance layers. In these examples, ε_p was kept to be 5 $\sim$ 10%. The features of these spectra are as follows: (A) ___ the cyclotron resonance layer was located on the inner side of the plasma crosssection - ΔT_i was medium and no high energy tail was present. (B) ___ the cyclotron resonance layer was located on the outer side of the plasma crosssection - ΔT_i was large and also no high energy tail was present. (C) ___ the cyclotron resonance layer was located on the outer edge of the plasma crosssection - ΔT_i was medium and remarkable high energy tail was built. Figure 6 compares temporal evolutions of count numbers of charge exchange neutrals at 1.5 KeV in these cases. The 1/e decay times of count numbers after terminating the rf pulse were (A) 0.7 ms, (B) 1.5 ms and (C) < 0.3 ms, respectively. This indicates that heating took place in the most central region in case B. It is consistent with the fact that the two-ion hybrid resonance layer was located most closely to the plasma center in case B, since the two-ion hybrid resonance layer lies on little high field side of the cyclotron resonance layer and strong wave damping occures near the two-ion hybrid resonance layer, following the mode conversion theory[10]. Figure 7 shows ion temperature increase ΔT_i divided by the rf net power as a function of the toroidal field ___ the position of the cyclotron resonance layer for hydrogen. The variation of T_i/P_{Net} is asymmetric with respect to the plasma center. The maximum $\Delta T_i/P_{Net}$ was obtained at $B_T \sim 18$ KG, which is consistent with that wave damping variation denotes a bottom at $B_T \sim 18$ KG as shown in Fig. 4. Next we examined the response of charge exchange neutral spectra to the ratio of proton to deuteron density ε_p, keeping the toroidal field at 18 KG and 16.4 KG. Figure 8 shows some examples of charge exchange neutral spectra for different values of ε_p. Here the toroidal field was fixed at 18 KG. Profiles of L_α lines of deuterium and hydrogen were measured with the monochromator for each case. They are also shown in Fig. 8, where curves are normalized at the peak corresponding to deuterium. ε_p was determined as

$$\varepsilon_p = \frac{\sqrt{2}\ P_H}{\alpha\ P_D} \quad ,$$

where P_D and P_H are peak values of L_α lines of deuterium and hydrogen, respectively, assuming same temperatures, and α is a correction factor for absorption effect of the deuterium L_α line by ground levels of deuterium. Rough calculation shows α is about 1.3 for the present experiment. We make ε_p simply to be obtained from P_H/P_D for convenience. This procedure includes error within 20%. The features of spectra shown in Fig. 8 are as follows:

(D) For $\varepsilon_p < 5\%$, a remarkable high energy tail was build and ΔT_i was medium.

(B) For $\varepsilon_p = 5 \sim 10\%$, a high energy tail disappeared and ΔT_i was large.

(E) For $\varepsilon_p > 10\%$, a high energy tail was also absent but ΔT_i was small.

A decay time of the high energy tail in case D was 1.2 ms, which was comparable with that of the bulk ion temperature 1.5 ms. In addition, the former is much longer than that of the high energy tail in case C, 0.3 ms. Figure 9 shows $\Delta T_i/P_{Net}$ as a function of ε_p. It can be concluded that the most favorable heating is realized at $\varepsilon_p = 5 \sim 10\%$ for $B_T = 18$ KG.

Radial profile of ion temperature in the case of $\varepsilon_p = 5 \sim 10\%$ and $B_T = 18$ KG was determined from the Doppler broadening of OVII (1623 Å), CV (2271 Å) and CIV (1548 Å) lines and from the localization of line intensities (Fig. 10). The localization of the impurity emissions was experimentally confirmed by measuring spatial distributions of their total line intensities. The spatial distributions of the total line emission coefficient were obtained by using an Abel inversion method from the radiances observed along different horizontal chords. For the central ion temperature, data from the charge exchange were adopted. Ion temperatures in the scrape-off layer were measured with the multigrid analyzer and the Katsumata probe. Ion heating in the overall plasma crosssection was shown in Fig. 10. Radial profiles of electron temperature and density are depicted in Fig. 11. Peripheral electron heating was observed. When ε_p was smaller than 5%, no electron heating occurred in the whole plasma crosssection.

2.4 Discussion

We consider power balances using the radial profiles shown in Figs. 10 and 11.

Steady state power balances for ions with and without the rf power are as follows.

$$Q'_{ei} + Q^i_{rf} - \frac{W'_i}{\tau'_{Ei}} = 0 \quad \text{with rf power} \qquad (1)$$

$$Q_{ei} - \frac{W_i}{\tau_{Ei}} = 0 \quad \text{without rf power} \quad , \tag{2}$$

where Q_{ei}, Q^i_{rf}, W_i and τ_{Ei} are power transferred from electrons to ions, the rf power to ions, energy of ions and ion energy confinement time, respectively, and (') denotes quantities with rf power. W_i, W'_i, Q_{ei} and Q'_{ei} are calculated from the radial profiles of $T_i(r)$, $T_e(r)$ and $n_e(r)$ shown in Figs. 10, 11, assuming same values of perpendicular and parallel temperatures. Those are tabulated in Table 1. The rf power to ions Q^i_{rf} can be estimated from

$$Q^i_{rf} = \frac{W'_i - W_i}{\tau_s} \quad .$$

Here τ_s is a decay time of bulk ion temperature after terminating the rf pulse, and was 1.5 ms (Fig. 2). Then, Q^i_{rf} = 38 KW. An ion heating efficiency η_i is defined as the ratio of Q^i_{rf} to the rf net power P_{Net}. The efficiency is about 40%. From Eq. (1) and (2) τ_{Ei} and τ'_{Ei} are calculated to be 4.8 ms and 3.7 ms, respectively. They are in agreement within experimental error (±25%).

Steady state power balances for electrons with and without the rf power are given below.

$$P_{OH} - Q'_{ei} + Q^e_{rf} - \frac{W'_e}{\tau'_{Ee}} = 0 \quad \text{with rf power} \tag{3}$$

$$P_{OH} - Q_{ei} - \frac{W_e}{\tau_{Ee}} = 0 \quad \text{without rf power} \ , \tag{4}$$

where P_{OH}, Q^e_{rf}, W_e and τ_{Ee} are the ohmic input power, the rf power to electrons, energy of electrons and electron energy confinement time, respectively. Values of P_{OH}, W_e and W'_e are shown in Table 1. Q^e_{rf} is unknown, since time evolution of electron temperature after terminating the rf pulse did not measured. τ_{Ee} and τ'_{Ee} are calculated to be 2.2 ms and 1.9 ms, respectively, assuming $Q^e_{rf} = 0$. Thus, the rf heating causes no change in the ion and electron energy confinements. The rest of the rf power presumably went to the edge plasma, although the detail has not yet been clarified.

2.5 Summary

(1) Rf net power was up to 140 KW. Rf net energy of 1 KJ was applied.

(2) No change of one turn loop voltage and electron density was observed.

(3) The maximum $\Delta T_i/P_{Net}$ was observed at B_T = 18 KG and ε_p = 5 ∿ 10%.

(i) Ion was heated in the overall plasma crosssection.

(ii) No high energy tail was built.

(iii) No adverse effect on the plasma confinement was observed.

(iv) Ion heating efficiency was about 40%.

3. Very High Efficiency Ion Heating Experiment

It was experimentally confirmed that divertor heat flux was roughly equal to the rf power irradiated to the plasma. The fact indicates that the rf power irradiated to a plasma is transformed to a kinetic energy of particles. In Sec. 2, however, heating efficiency was only 40%. The rest of the rf power went to the edge plasma by an electrostatic coupling between the antenna and the plasma surrounding it. In addition the antenna loading impedance R_s (6 ∿ 8Ω) was considerably high for a wave coupling without high Q toroidal eigen mode.

3.1 Improvements

To avoid the electrostatic coupling, we installed a Faraday shield[16] closely over the ceramic cover (Fig. 12). The Faraday shield was made of molybdenum strips (5 mm azimuthally × 1 mm radially, separated by a 5 mm gap) and U-shaped stainless steel covers which surrounded back and side surfaces of the ceramic cover and had two gaps azimuthally. The ends of the strips were connected to the stainless steel covers, which were terminated to the shells.

One of the other problems associated with ICRF heating experiment was rf breakdown. It occurred at the antenna and the power feed-through insulator. In order to prevent rf breakdown, the antenna cleaning was performed by supplying the rf power in the absence of the plasma and generating rf discharges. If they did not occur, the rf power was raised gradually till they began to occur again. These procedures were continued up to a desirable rf current level. In the previous experiment, the end of the antenna was terminated to the vacuum vessel. This time we connected $\sim \frac{\lambda}{2}$ coaxial cable with an adjustable short-circuit end, and set the midpoint

2.5 Summary

(1) Rf net power was up to 140 KW. Rf net energy of 1 KJ was applied.

(2) No change of one turn loop voltage and electron density was observed.

(3) The maximum $\Delta T_i/P_{Net}$ was observed at B_T = 18 KG and $\varepsilon_p = 5 \sim 10\%$.

(i) Ion was heated in the overall plasma crosssection.

(ii) No high energy tail was built.

(iii) No adverse effect on the plasma confinement was observed.

(iv) Ion heating efficiency was about 40%.

3. Very High Efficiency Ion Heating Experiment

It was experimentally confirmed that divertor heat flux was roughly equal to the rf power irradiated to the plasma. The fact indicates that the rf power irradiated to a plasma is transformed to a kinetic energy of particles. In Sec. 2, however, heating efficiency was only 40%. The rest of the rf power went to the edge plasma by an electrostatic coupling between the antenna and the plasma surrounding it. In addition the antenna loading impedance R_s ($6 \sim 8\Omega$) was considerably high for a wave coupling without high Q toroidal eigen mode.

3.1 Improvements

To avoid the electrostatic coupling, we installed a Faraday shield[16] closely over the ceramic cover (Fig. 12). The Faraday shield was made of molybdenum strips (5 mm azimuthally × 1 mm radially, separated by a 5 mm gap) and U-shaped stainless steel covers which surrounded back and side surfaces of the ceramic cover and had two gaps azimuthally. The ends of the strips were connected to the stainless steel covers, which were terminated to the shells.

One of the other problems associated with ICRF heating experiment was rf breakdown. It occurred at the antenna and the power feed-through insulator. In order to prevent rf breakdown, the antenna cleaning was performed by supplying the rf power in the absence of the plasma and generating rf discharges. If they did not occur, the rf power was raised gradually till they began to occur again. These procedures were continued up to a desirable rf current level. In the previous experiment, the end of the antenna was terminated to the vacuum vessel. This time we connected $\sim \frac{\lambda}{2}$ coaxial cable with an adjustable short-circuit end, and set the midpoint

of the antenna to be a voltage null point. The voltage at the power feed-through was reduced to 50% for the same rf input power.

By means of above mentioned improvements, the antenna current has increased by a factor of 2, suggesting effective rf power which absorbed by ions has become about 4 times higher than in the previous experiment described in Sec. 2.

3.2 Results

Discharge conditions were almost same as those described in subsection 2.2. The toroidal field was 17.5 KG and the proton-to-deuteron density ratio was 8 ∿ 9%.

Figure 13 shows time evolution of ion temperature measured with the charge exchange neutral energy analyzer. It is shown that ion temperature increased from 160 eV to 430 eV by application of 180 KW rf net power including the circuit loss. Charge exchange neutral spectra sampled from 11 to 12 ms are shown in Fig. 14. Ion temperature is determined from the linear part of the spectra up to the neutral energy of 1.6 KeV. A significant amount (15%) of slightly higher energy component (∿750 eV) is present. The decay time of charge exchange count numbers after terminating the rf pulse has the same order for the energy range up to ∿4 KeV. Radial profiles of ion temperature were measured with the technique described in Sec. 2 (Fig. 15). Unfortunately, those of electron temperature were not observed in the present experiment. However, comparing Fig. 11 and Fig. 15, it is found that ion temperature exceeded electron temperature over the whole plasma crosssection.

The antenna loading impedance was reduced to 2.5 ∿ 3Ω, while one related to the circuit loss was 0.7 ∿ 0.8Ω. Then, the effective rf power P_{eff} which was irradiated to the plasma was about 130 ∿ 140 KW. On the other hand, the increase of ion energy was calculated to be about 140 Joule. The e-folding decay time of ion temperature after terminating the rf pulse was about 1 ms. Then, the rf power absorved by ions Q_{rf}^{i} is roughly estimated to be 140 KW (see subsection 2.4). It can be concluded that ion heating efficiency ($\equiv Q_{rf}^{i}/P_{eff}$) was raised up to 100% by means of the Faraday shield.

Figure 16 summarized ΔT_i, increase of central ion temperature, for various values of squares of the antenna current or P_{eff}, assuming the loading impedance to be 2Ω. The solid line shows ΔT_i versus sum of loss power

densities due to the neoclassical thermal conduction and the heat transfer from ions (electrons) to electrons (ions), assuming the plateau regime with the same coefficient as that obtained in the ohmically heated plasmas[1] and the central electron temperature of 300 eV. A scale of the loss power density is adjusted so that ◉ is put on the solid line. The figure shows that the other data points are well on the solid line. It can be concluded that the main loss mechanisms of the rf heated ions are the neoclassical thermal conduction and the electron-ion coupling. The ion energy confinement time during the heating phase estimated from the decay time of the bulk ion temperature is 1.9 ms in the case of P_{eff} = 140 KW, while one without heating is 4.8 ms. The reduction is explained by the neoclassical scaling (plateau regime) of the ion energy confinement time $\tau_{Ei} \propto T_i^{-3/2}$, since the loss power density due to the neoclassical thermal diffusion is about 6 times larger than that due to the electron-ion coupling. Figure 16 also shows that (the loss power dinsity)/ $P_{eff} \simeq 1\ W \cdot cm^{-3}$ / 10 KW. From this, a mean radius of the rf power deposition profle r_M is estimated to be $\sim$3 cm, which is consistent with that heating takes place in the central core of the plasma as described in Sec. 2.

4. Concluding Remarks

ICRF heating experiment using 2 ω_{CD} frequency for a deuteron plasma with a minority proton component was performed under the extremely pure wall condition ($Z_{eff} \simeq 1$). Optimum heating conditions were surveyed, varying the toroidal magnetic field B_T and the proton-to-deuteron density ratio ε_p. The most favorable ion heating was observed for the case of $B_T \sim 18$ KG and $\varepsilon_p = 5 \sim 10\%$. Heating efficiency, however, was only up to 40%. The rest of the rf power went to the edge plasma by an electrostatic coupling between the antenna and the plasma surrounding it.

In the next step, the antenna was electrostatically shielded by the full Faraday shield. The antenna loading impedance was reduced to less than 50%. Ion heating efficiency increased to about 100%. With the improvements against the rf breakdown, the rf net power of up to 180 KW was supplied. The effective rf power absorbed by ions reached 7 times of the Joule input into ions without the rf power. Ion temperature increased from 160 eV to 430 eV. Ion temperature exceeded electron temperature over the whole plasma crosssection. The loss mechanisms of the rf heated ions are explained by the neoclassical thermal conduction and electron-ion

densities due to the neoclassical thermal conduction and the heat transfer from ions (electrons) to electrons (ions), assuming the plateau regime with the same coefficient as that obtained in the ohmically heated plasmas[1] and the central electron temperature of 300 eV. A scale of the loss power density is adjusted so that ◉ is put on the solid line. The figure shows that the other data points are well on the solid line. It can be concluded that the main loss mechanisms of the rf heated ions are the neoclassical thermal conduction and the electron-ion coupling. The ion energy confinement time during the heating phase estimated from the decay time of the bulk ion temperature is 1.9 ms in the case of P_{eff} = 140 KW, while one without heating is 4.8 ms. The reduction is explained by the neoclassical scaling (plateau regime) of the ion energy confinement time $\tau_{Ei} \propto T_i^{-3/2}$, since the loss power density due to the neoclassical thermal diffusion is about 6 times larger than that due to the electron-ion coupling. Figure 16 also shows that (the loss power dinsity)/ $P_{eff} \simeq 1\ W \cdot cm^{-3}$ / 10 KW. From this, a mean radius of the rf power deposition profle r_M is estimated to be $\sim$3 cm, which is consistent with that heating takes place in the central core of the plasma as described in Sec. 2.

4. Concluding Remarks

ICRF heating experiment using 2 ω_{CD} frequency for a deuteron plasma with a minority proton component was performed under the extremely pure wall condition ($Z_{eff} \simeq 1$). Optimum heating conditions were surveyed, varying the toroidal magnetic field B_T and the proton-to-deuteron density ratio ε_p. The most favorable ion heating was observed for the case of $B_T \sim 18$ KG and $\varepsilon_p = 5 \sim 10\%$. Heating efficiency, however, was only up to 40%. The rest of the rf power went to the edge plasma by an electrostatic coupling between the antenna and the plasma surrounding it.

In the next step, the antenna was electrostatically shielded by the full Faraday shield. The antenna loading impedance was reduced to less than 50%. Ion heating efficiency increased to about 100%. With the improvements against the rf breakdown, the rf net power of up to 180 KW was supplied. The effective rf power absorbed by ions reached 7 times of the Joule input into ions without the rf power. Ion temperature increased from 160 eV to 430 eV. Ion temperature exceeded electron temperature over the whole plasma crosssection. The loss mechanisms of the rf heated ions are explained by the neoclassical thermal conduction and electron-ion

coupling.

The results can be applied to a D-T reactor. Ions are heated in a D-T plasma by adding small amount of hydrogen, since D-H ion hybrid effects still hold true for a H+D+T mixture plasma. We simulated this scheme using a $H+D+H_e^3$ (roughly 0.2:1:1) plasma. Similar asymmetry shown in Fig. 4 was observed with respect to the variation of wave amplitude versus major radius location of a fundamental cyclotron resonance layer of proton. Ion temperature increased from 230 eV to 265 eV in application of the rf net power of 90 KW. The result will be improved reducing the proton-to-deuteron density ratio to less than 10%. Electron heating is also expected for a D-T(1:1) plasma according to the mode conversion theory[10].

In DIVA, a power density of 1.4 $W \cdot cm^{-3}$ has been reached without any deleterious effects, which is seven times higher than 30 MW in Intor. Recently, an all metal antenna was successfully employed in TFR[17]. In a reactor, a ceramic spacer cannot be used due to neutron damage. The results encourage us to extend ICRF heating to a reactor plasma, since a coupling structure can be made of same material as a first wall or a neutralizer plate of a reactor.

Acknowledgement

We would like to thank Mr. K. Anno and his groups for their operation of DIVA and support in construction of the rf generator. We would also like to express our gratitude to Drs. Y. TANAKA, Y. OBATA and S. MORI for their continuous encouragement.

coupling.

The results can be applied to a D-T reactor. Ions are heated in a D-T plasma by adding small amount of hydrogen, since D-H ion hybrid effects still hold true for a H+D+T mixture plasma. We simulated this scheme using a H+D+H_e^3 (roughly 0.2:1:1) plasma. Similar asymmetry shown in Fig. 4 was observed with respect to the variation of wave amplitude versus major radius location of a fundamental cyclotron resonance layer of proton. Ion temperature increased from 230 eV to 265 eV in application of the rf net power of 90 KW. The result will be improved reducing the proton-to-deuteron density ratio to less than 10%. Electron heating is also expected for a D-T(1:1) plasma according to the mode conversion theory[10].

In DIVA, a power density of 1.4 $W \cdot cm^{-3}$ has been reached without any deleterious effects, which is seven times higher than 30 MW in Intor. Recently, an all metal antenna was successfully employed in TFR[17]. In a reactor, a ceramic spacer cannot be used due to neutron damage. The results encourage us to extend ICRF heating to a reactor plasma, since a coupling structure can be made of same material as a first wall or a neutralizer plate of a reactor.

Acknowledgement

We would like to thank Mr. K. Anno and his groups for their operation of DIVA and support in construction of the rf generator. We would also like to express our gratitude to Drs. Y. TANAKA, Y. OBATA and S. MORI for their continuous encouragement.

References

1) DIVA GROUP, Nucl. Fusion 18 (1978) 1619.
2) IVANOV, N.V., KOVAN, I.A., LOS', E.V., JETP Lett. 14 (1971) 138.
3) VDOVIN, V.L., ZINOV'EV, O.A., IVANOV, A.A., KOZOROVITSKII, L.L., PARAIL, V.V., et al., JETP Lett. 14 (1971) 149.
4) HOOKE, W.M., HOSEA, J.C., in Controlled Fusion and Plasma Physics (Proc. 5th Europ. Conf., Grenoble, 1972) Vol.1, (1972) 107; HOSEA, J.C., HOOKE, W.M., Phys. Rev. Lett., 31 (1973) 150; ADAM, J., CHANCE, M., EUBANK, H., GETTY, W., HINNOV, E., et al., in Plasma Physics and Controlled Nuclear Fusion Research (Proc. 5th Int. Conf., Tokyo, 1974) Vol.2, IAEA, Vienna (1975) 65.
5) TFR-GROUP, Proc. 3rd Int. Meeting on Theo. and Exp. Aspects of Heating Toroidal Plasmas, Grenoble, 1976, Vol.1, (1976) 87; TFR-GROUP, in Plasma Physics and Controlled Nuclear Fusion Research (Proc. 6th Int. Conf., Berchtesgaden, 1976) Vol.3, (1977) 39.
6) VDOVIN, V.L., SHAPOTKOVSKII, N.V., RUSANOV, V.D., Proc. 3rd Int. Meeting on Theo. and Exp. Aspects of Heating Toroidal Plasmas, Grenoble, 1976, Vol.2, (1976) 349.
7) BUZANKIN, V.V., VERSHKOV, V.A., IVANOV, N.V., KOVAN, I.A., KRUPIN, V.A., et al., in Plasma Physics and Controlled Nuclear Fusion Research (Proc. 6th Int. Conf., Berchtesgaden, 1976) Vol.3, (1977) 61.
8) TAKAHASHI, H., DAUGHNEY, C.C., ELLIS, Jr., R.A., GOLDSTON, R.M., HSUAN, H., et al., Phys. Rev. Lett. 39 (1977) 31.
9) JACQUINOT, J. MCVEY, B.D., SCHARER, J.E., Phys. Rev. Lett. 39 (1977) 88.
10) PERKINS, F.W., Nucl. Fusion 17 (1977) 1197.
11) TAKAHASHI, H., ICRF Heating in Tokamaks, Princeton Plasma Physics Lab. Report, PPPL-1374 (1978).
12) TFR-GROUP, Proc. of Joint Varenna-Grenoble Int. Symp. on Heating in Toroidal Plasmas, Grenoble (1978).
13) SUGIE, T., TAKEUCHI, H., KASAI, S., FUNAHASHI, A., TAKAHASHI, K., KIMURA, H., J. Phys. Soc. Japan, 44 (1978) 1960.
14) KIMURA, H., ODAJIMA, K., SUGIE, T., MAEDA, H., Application of Multigrid Energy Analyzer to the Scrape-off Layer Plasma in DIVA, to be published in Japan J. Appl. Phys.
15) ODAJIMA, K., KIMURA, H., MAEDA, H., OHASA, K., Japan J. Appl. Phys. 17 (1978) 1281.
16) ROTHMAN, M.A., SINCLAIR, R.M., YOSHIKAWA, S., Plasma Physics 8 (1966) 241.

17) TRF GROUP, EUR-CEA-FC-988 (1979).

18) DIVA GROUP, J. Varenna-Grenoble Inter. Symp. (Grenoble 1978) II (1978).

Table 1 Power balances with and without the rf power.
$P_{OH} \simeq 85$ kW, $P_{Net} \simeq 100$ kW, $\varepsilon_p = 5 \sim 10\%$, $B_T = 18$ KG.

W_e	W_i	Q_{ei}	τ_{Ee}	τ_{Ei}					WITHOUT RF
141 Joule	95 Joule	20 kW	2.2 ms	4.8 ms					
W'_e	W'_i	Q'_{ei}	τ'_{Ee}	τ'_{Ei}	Q^e_{rf}	Q^i_{rf}	η_e	η_i	WITH RF
158 Joule	151 Joule	3 kW	$\leqslant$ 1.9 ms	3.7 ms	?	38 kW	?	$\sim$40 %	

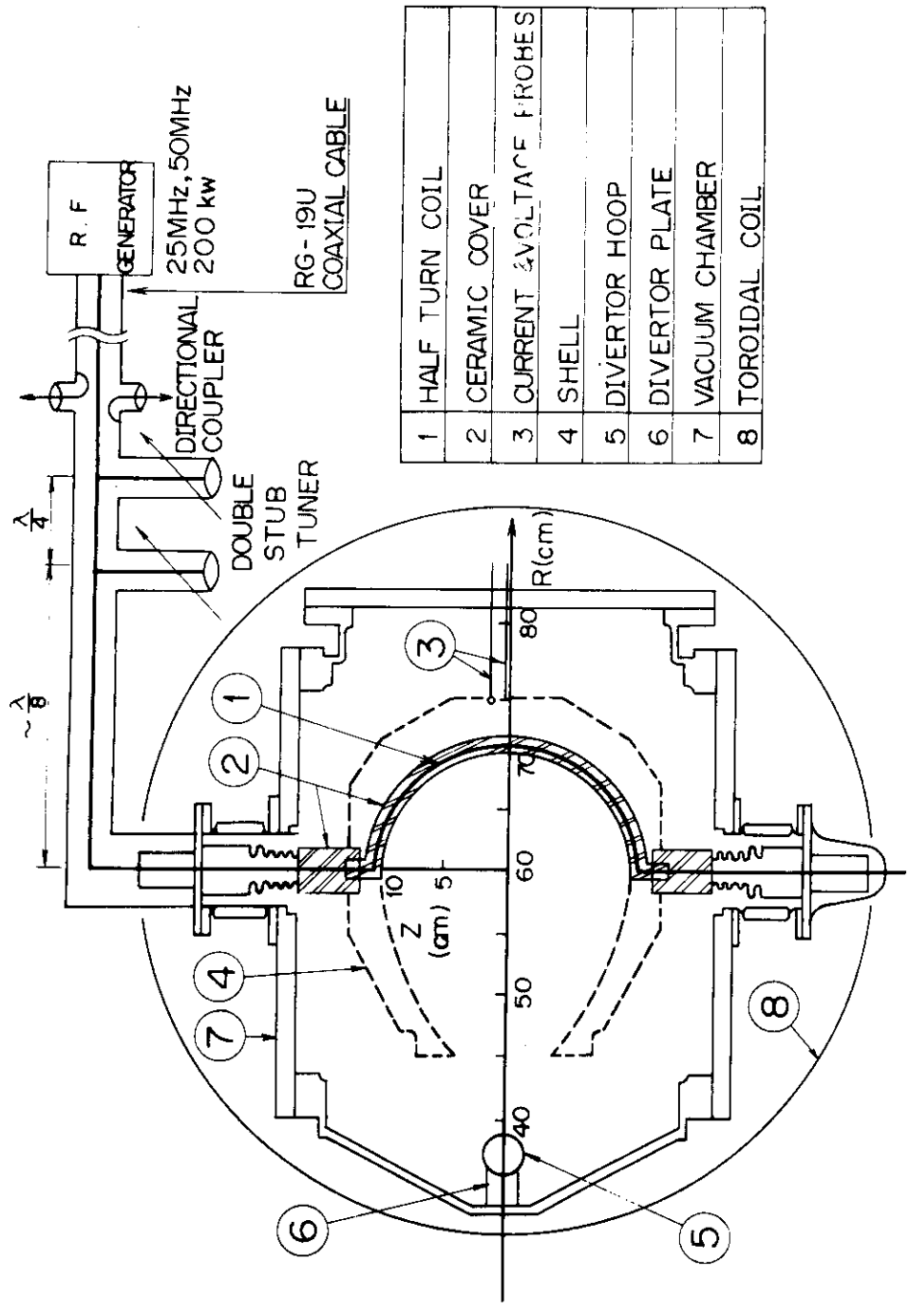

Fig. 1 Cross-sectional view of DIVA together with a launching structure (antanna), a matching network and a transmission line.

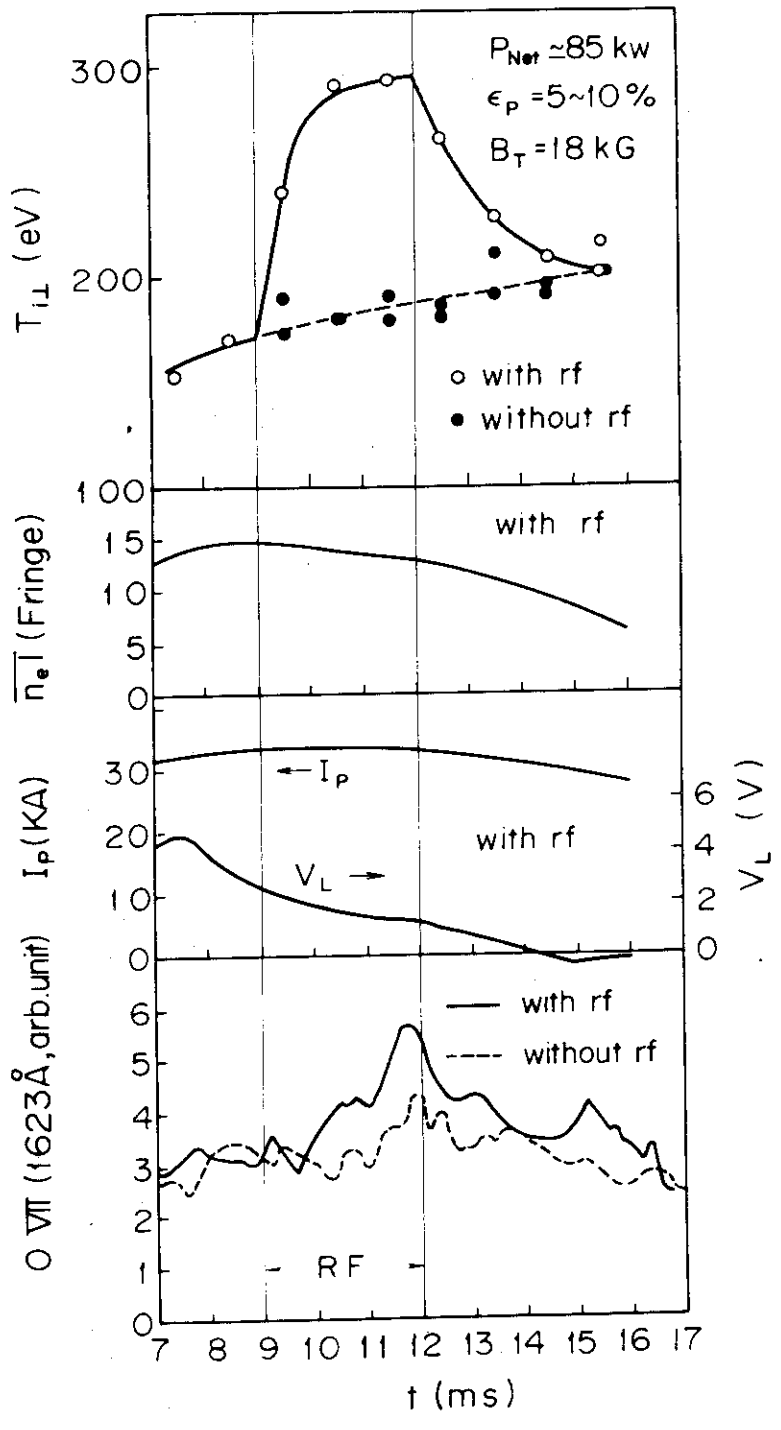

Fig. 2 Time evolutions of perpendicular ion temperature $T_{i\perp}$(CX), electron line density $\overline{n_e l}$, plasma current I_p, one turn loop voltage V_L and spectral line intensity OVII (1623 Å).

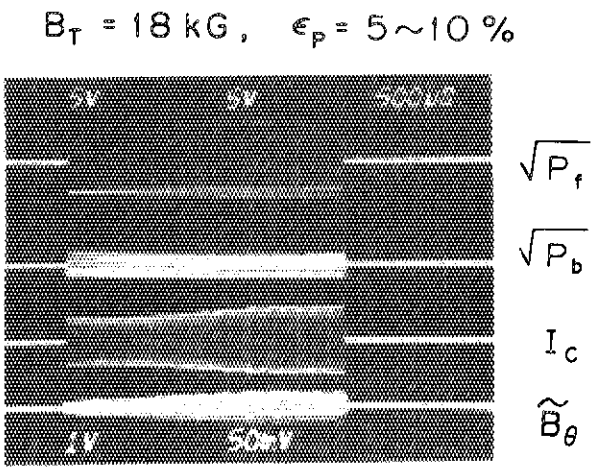

Fig. 3 Typical signals of square roots of incident and reflected rf powers $\sqrt{P_f}$, $\sqrt{P_r}$, coil current I_C and magnetic fluctuation $\tilde{B}_\theta$.

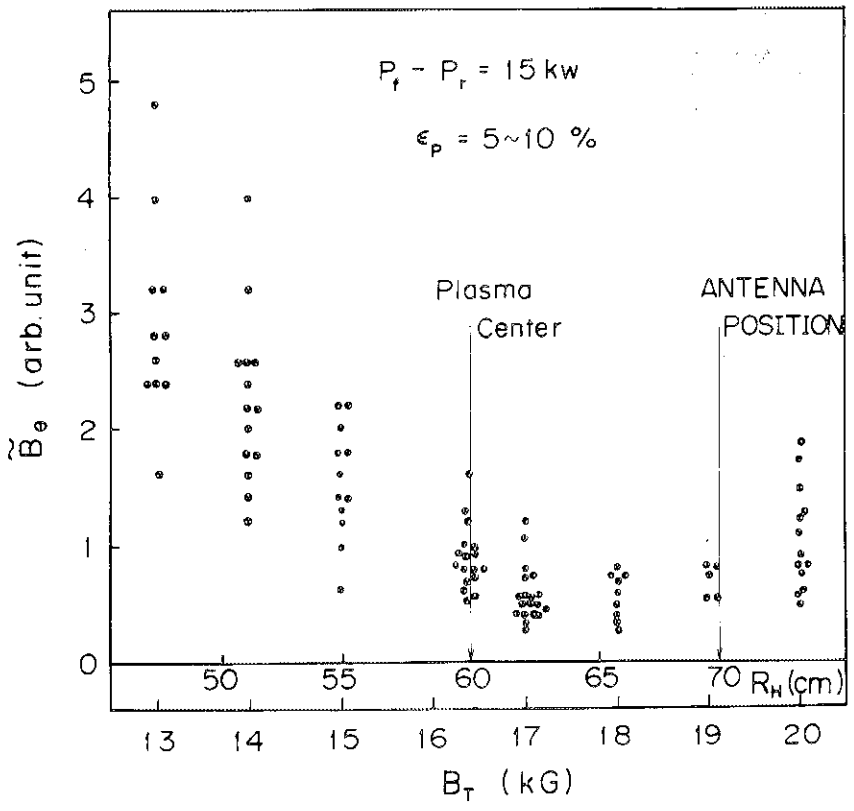

Fig. 4 Magnetic fluctuation $\tilde{B}_\theta$ as a function of the toroidal field B_T or the major radius location of a fundamental cyclotron resonance layer for hydrogen R_H. The frequency was fixed at 25 MHz and ϵ_p = 5 ∿ 10%.

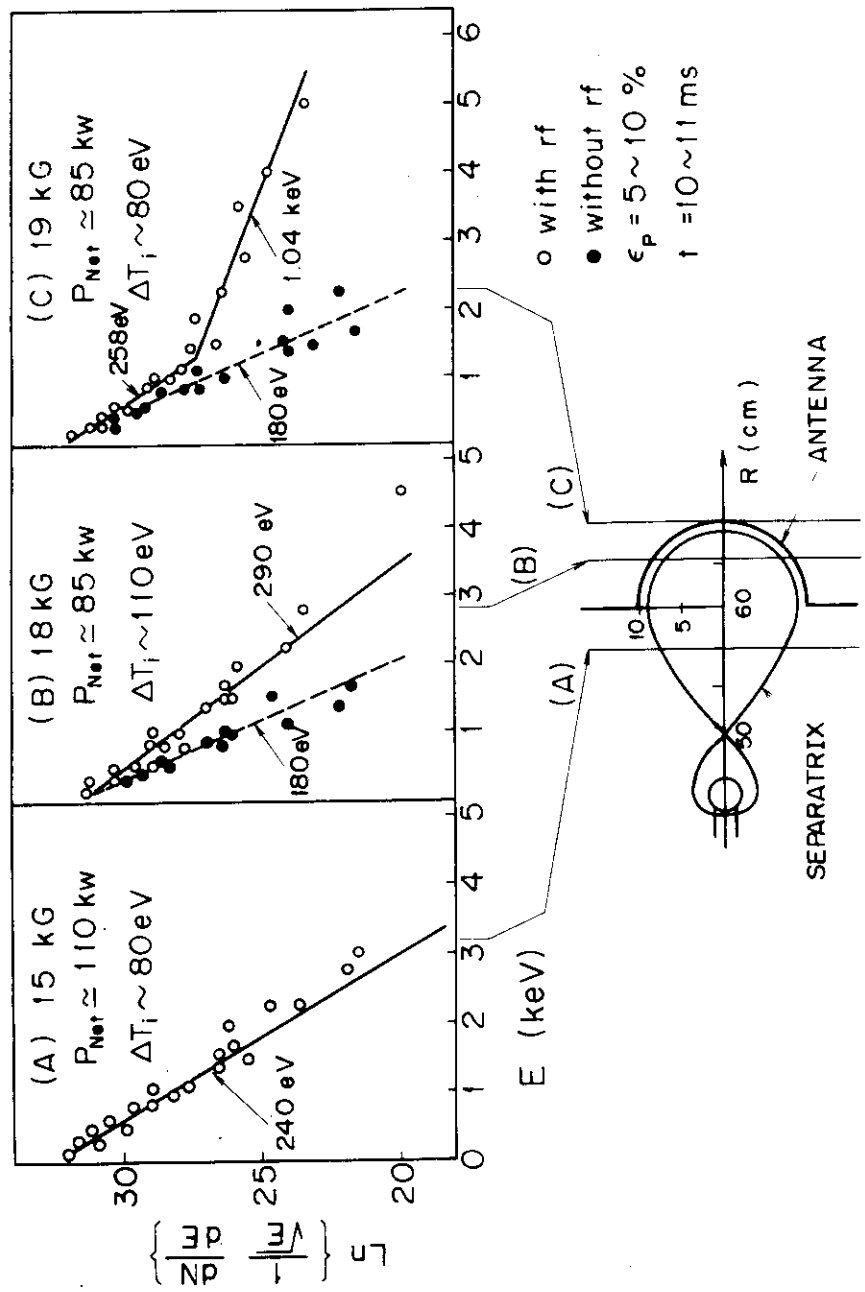

Fig. 5 Charge exchange neutral spectra for different toroidal fields and corresponding fundamental cyclotron resonance layers for hydrogen. ε_p was kept to be 5 ∿ 10%.

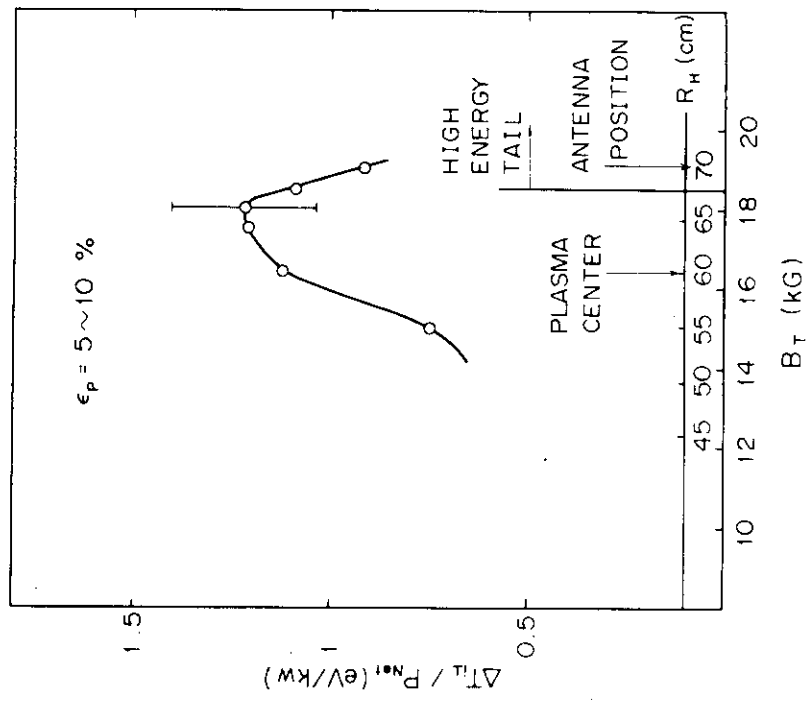

Fig. 7 Increase of ion temperature per unit rf net power versus the toroidal field or the position of the cyclotron resonance layer for hydrogen. ε_p was kept to be 5 ∿ 10%.

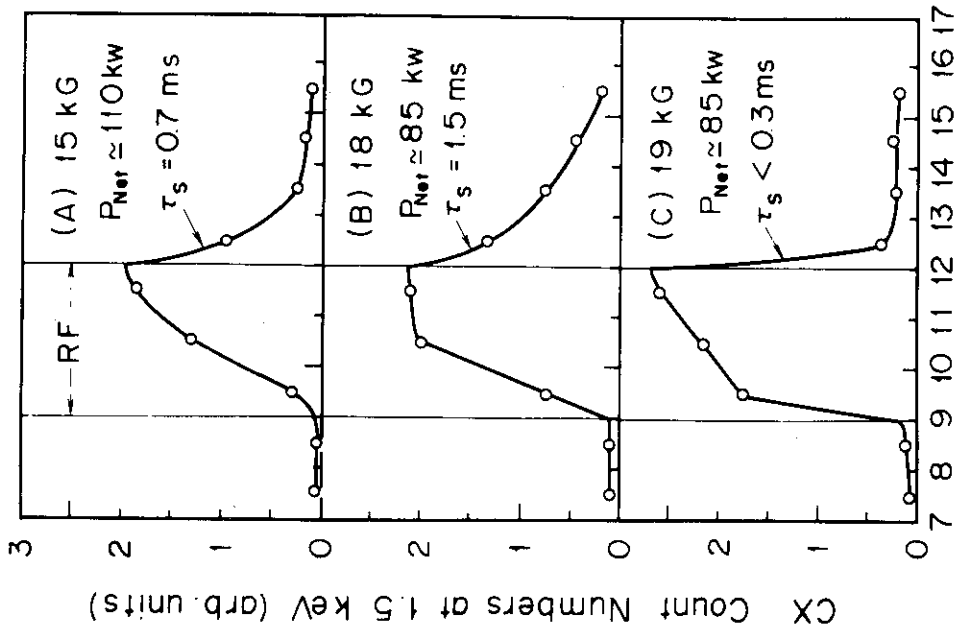

Fig. 6 Temporal evolutions of count numbers of charge exchange neutrals at 1.5 keV corresponding to the spectra shown in Fig. 5.

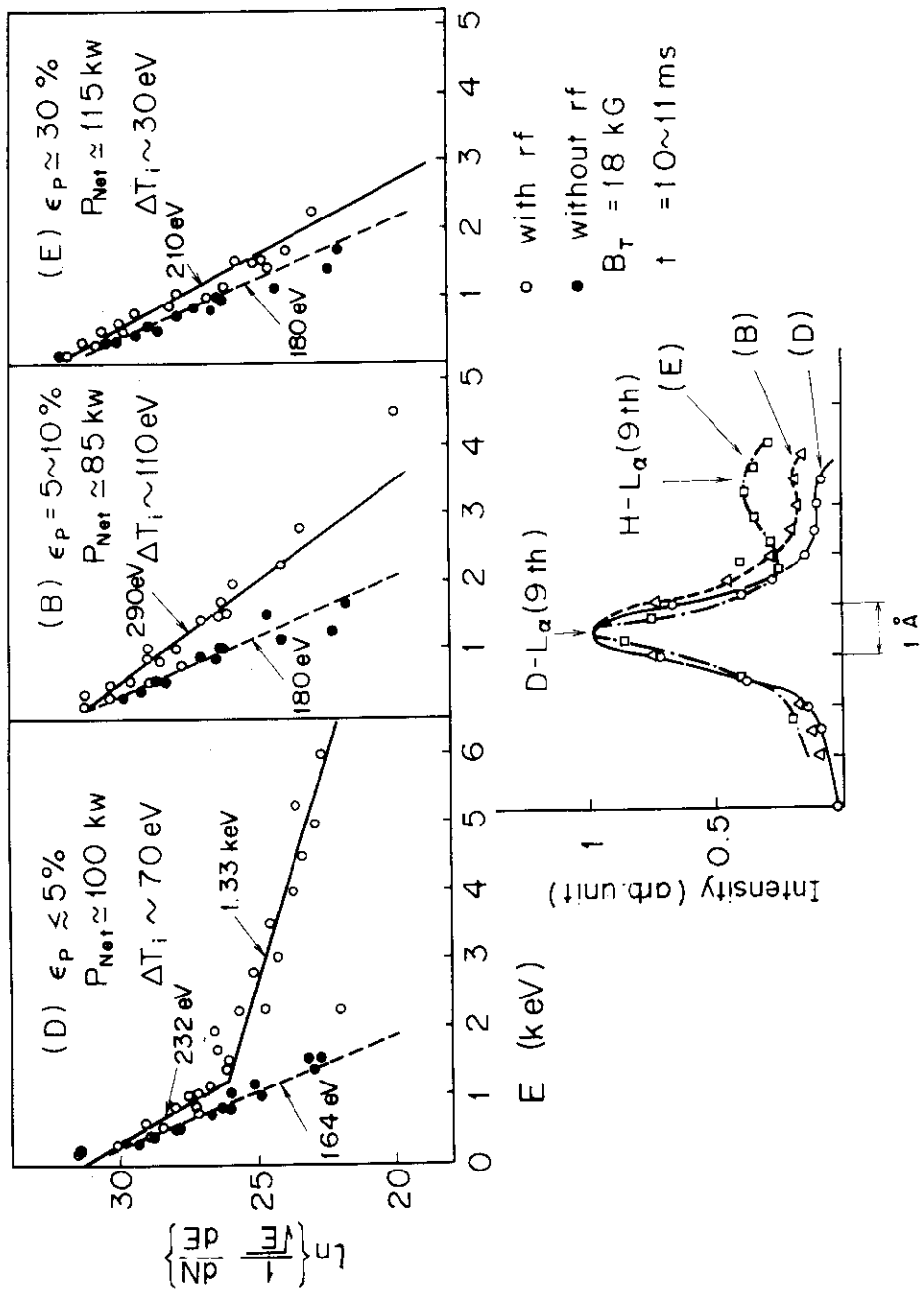

Fig. 8 Charge exchange neutral spectra for different values of ε_p and corresponding profiles of L_α lines of deuterium and hydrogen. The toroidal field was fixed at 18 KG.

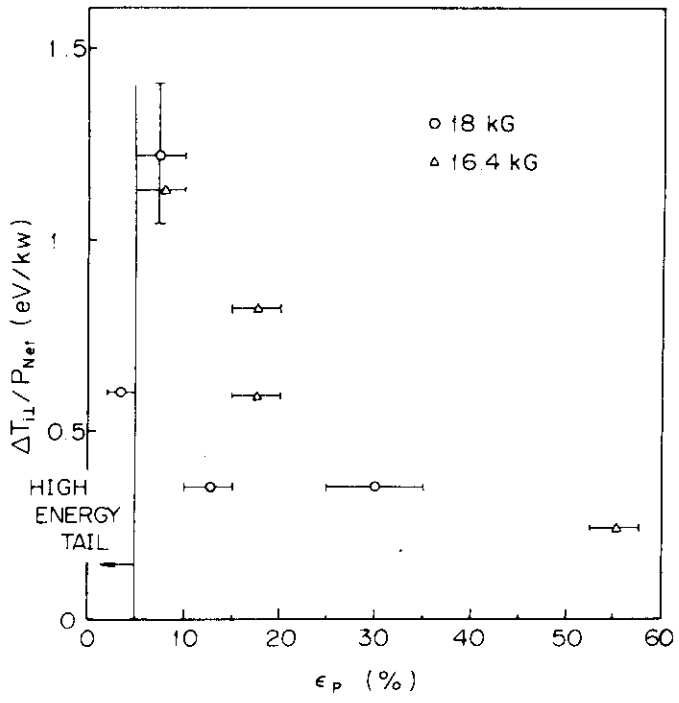

Fig. 9 Increase of ion temperature per unit rf net power as a function of ε_p. The toroidal field was fixed at 18 kG and 16.4 kG.

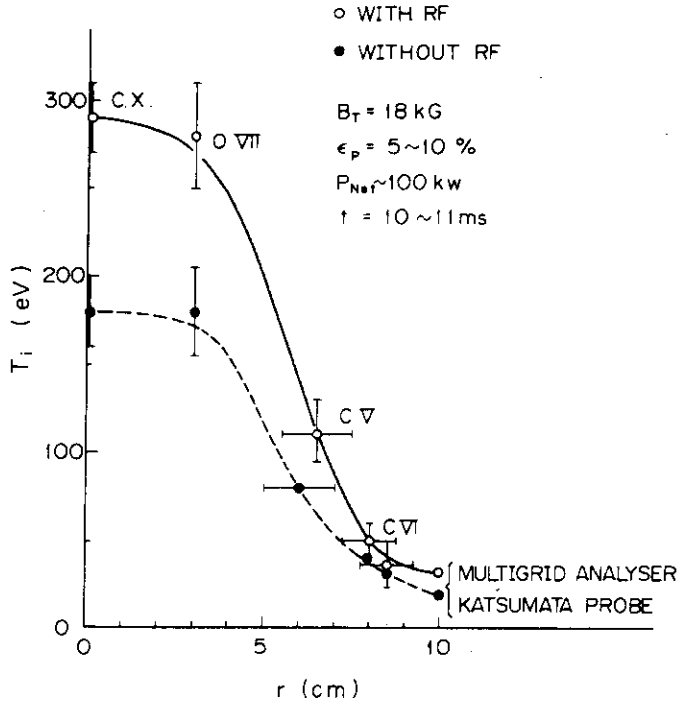

Fig. 10 Radial profiles of ion temperature with and without rf power in the case of ε_p = 5 ∿ 10% and B_T = 18 kG.

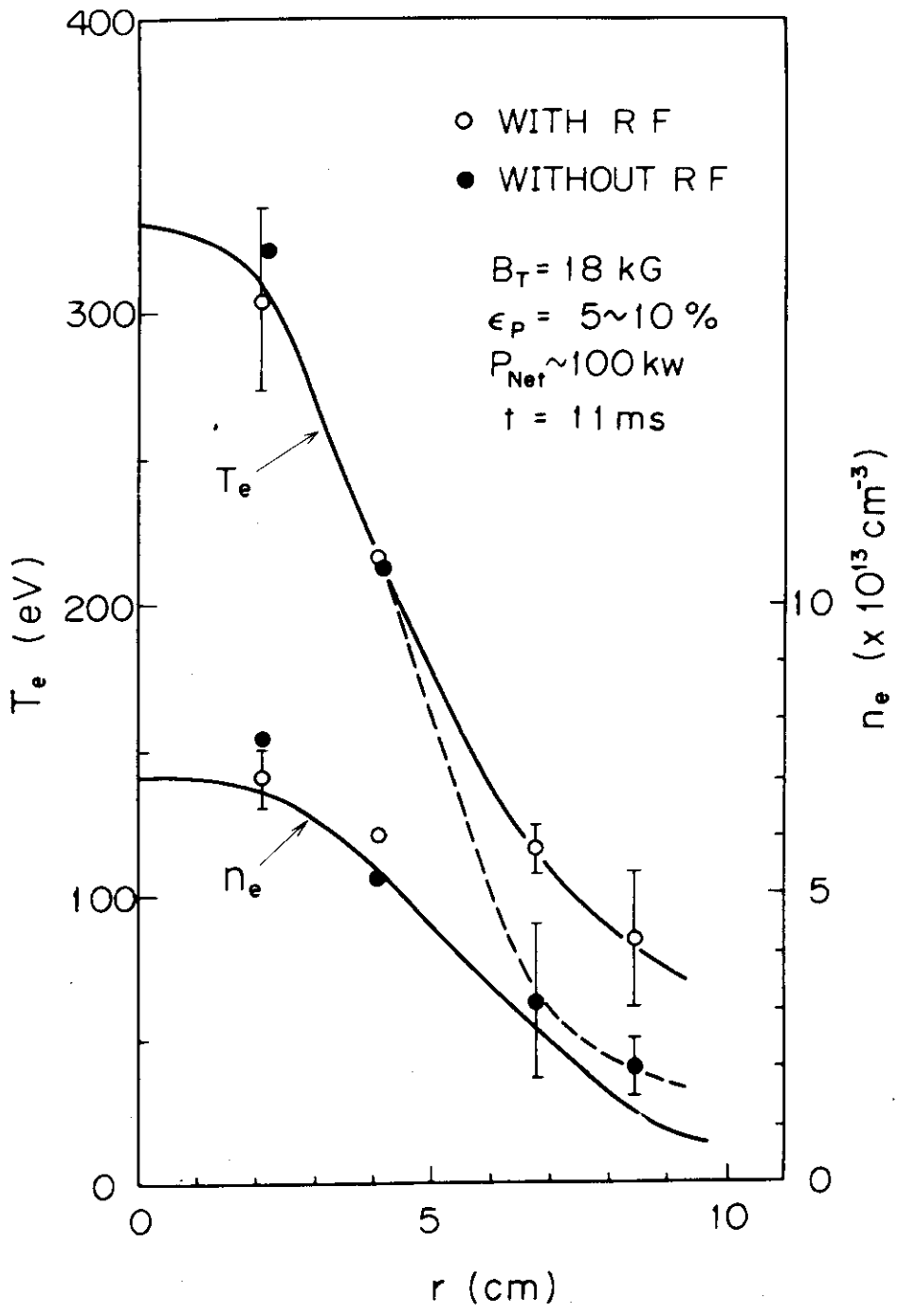

Fig. 11 Radial profiles of electron temperature and density with and without rf power in the case of ε_p = 5 ∿ 10%, B_T = 18 kG.

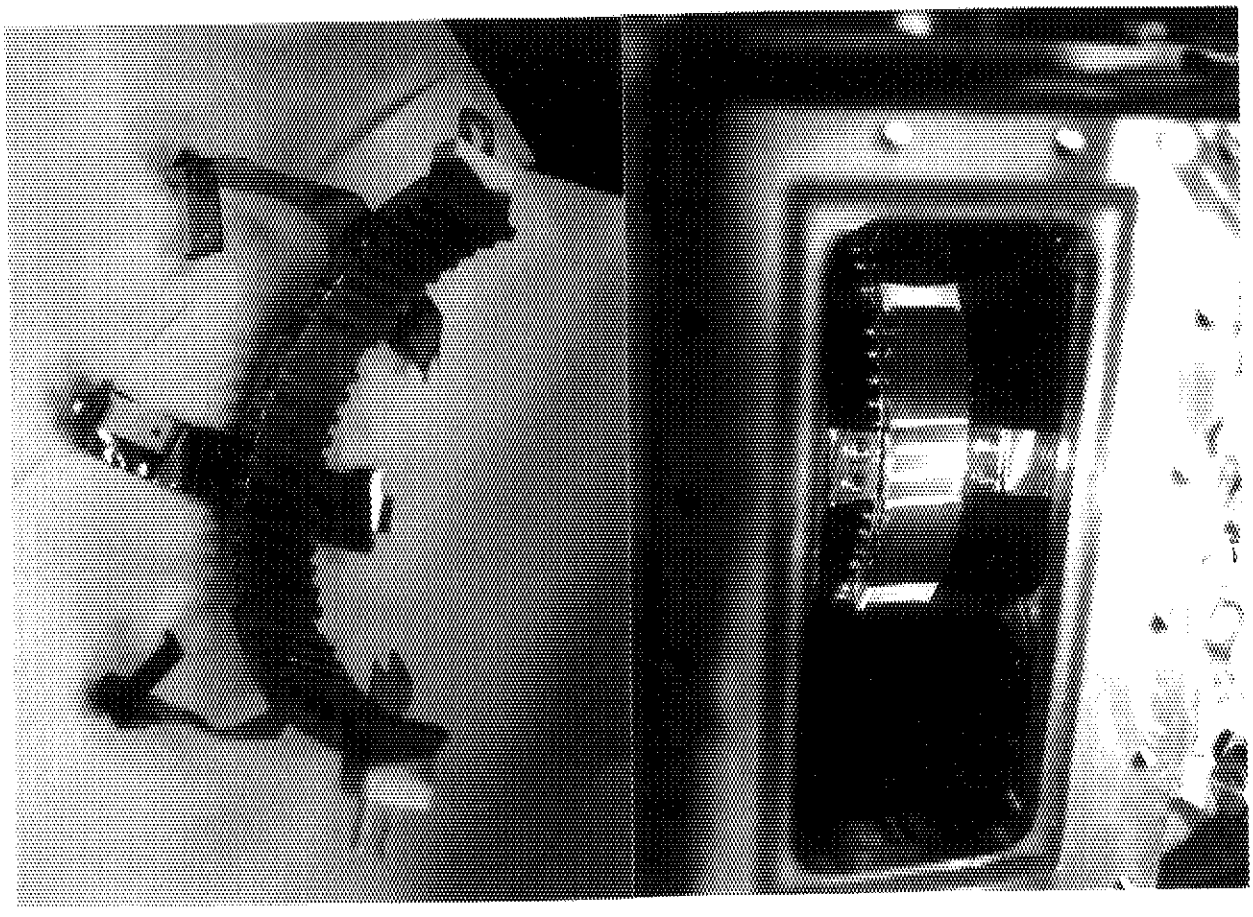

Fig. 12 Photograph of the antenna ceramic cover with the Faraday shield.

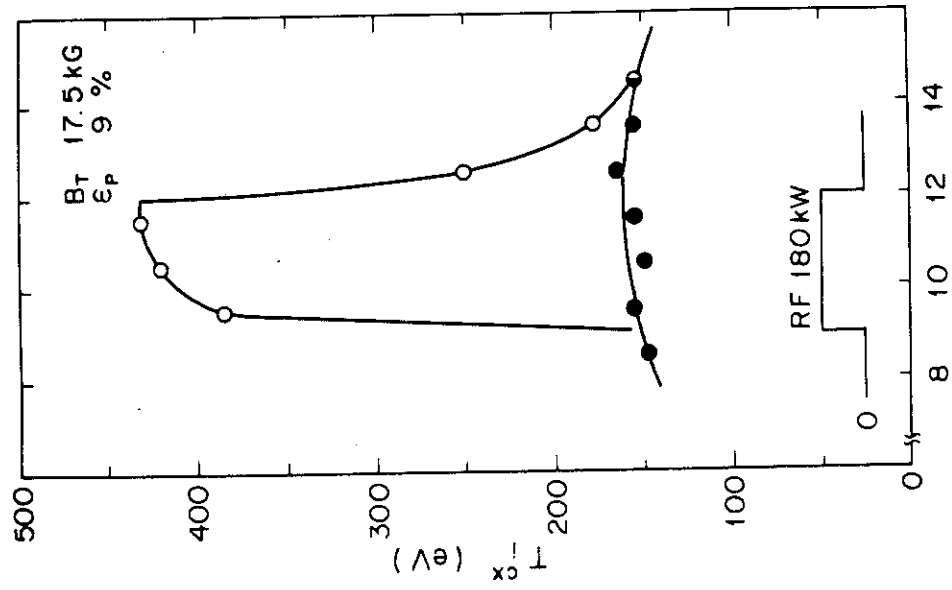

Fig. 13 Time evolutions of perpendicular ion temperature (CX).
○with rf heating, ●without rf heating.

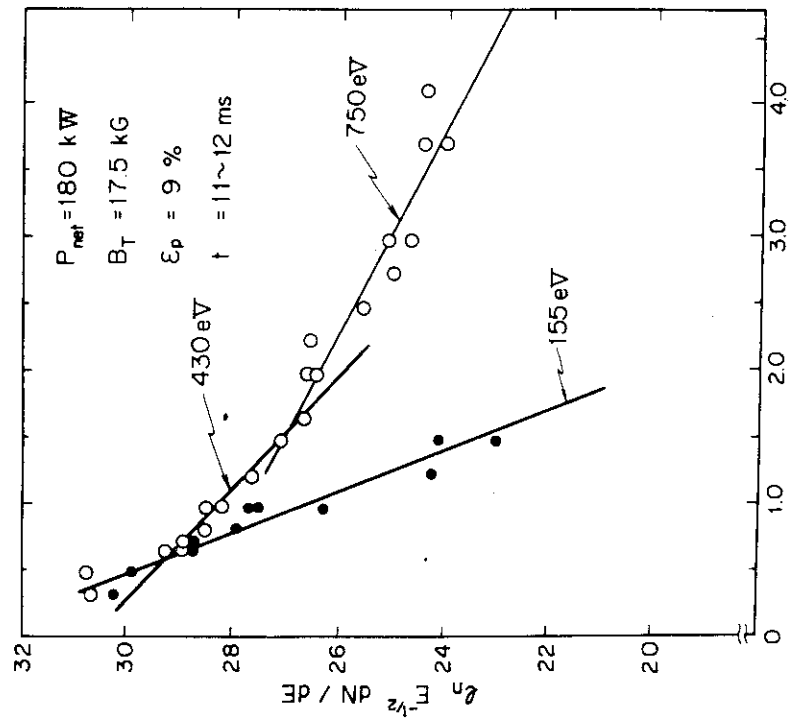

Fig. 14 Energy spectra of charge exchange neutrals.
○with rf heating, ●without rf heating.

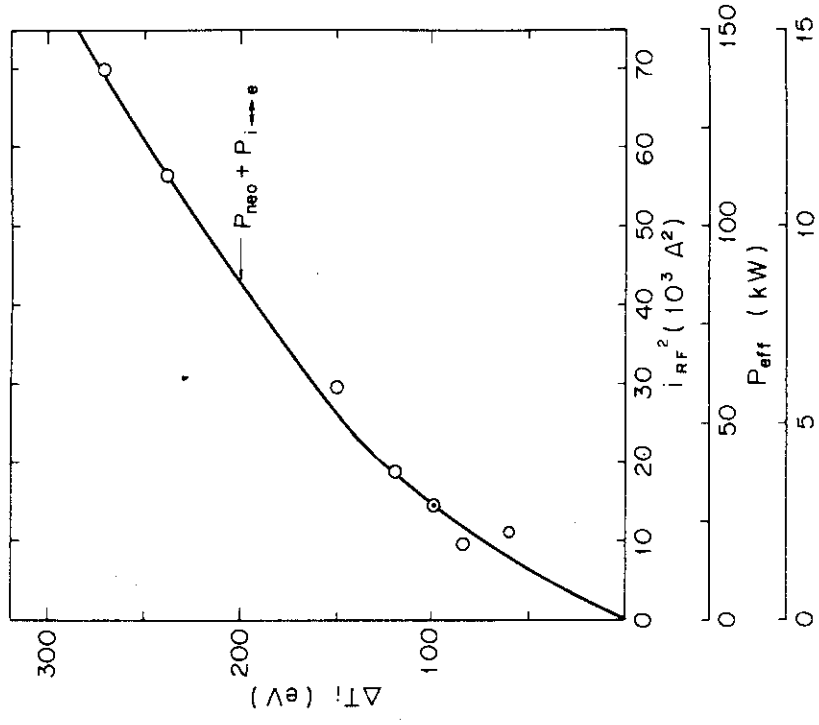

Fig. 16 Central ion temperature increase ΔT_i versus squares of antenna current i_{RF}^2 or effective rf power P_{eff} irradiated to the plasma. The solid line shows calculation of ΔT_i versus sum of loss power densities due to neoclassical thermal conduction and electron-ion coupling. A scale of the loss power densities is adjusted so that ◉ is put on the solid line.

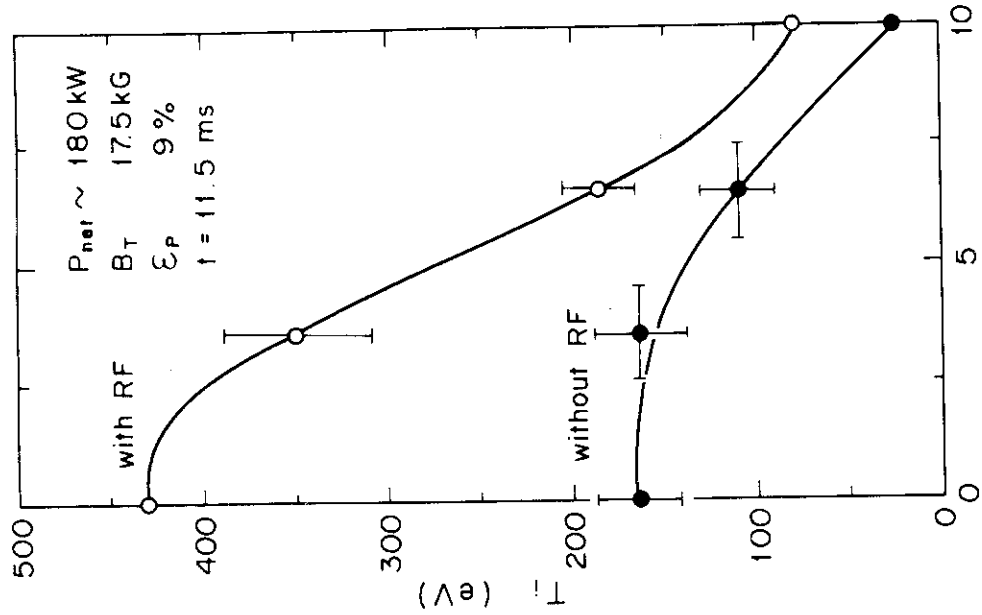

Fig. 15 Radial profiles of ion temperature, measured with the technique described in Sec. 2.